Influences of polypropylene grafted to SiO_2 nanoparticles on the crystallization behavior and mechanical properties of polypropylene/SiO_2 nanocomposites

Masaki Umemori, Toshiaki Taniike and Minoru Terano*

School of Materials Science, Japan Advanced Institute of Science and Technology, 1-1 Asahidai, Nomi, Ishikawa, 923-1211, Japan

Fax: (+81)761 51 1625; E-mail: terano@jaist.ac.jp

Abstract

Influences of polypropylene (PP) grafted to SiO_2 nanoparticles (7 nm) were studied on the crystallization behavior and the mechanical properties of PP/SiO_2 nanocomposites. PP for the matrix and grafting was synthesized in order to have an identical primary structure, aiming at their co-crystallization and resulting reinforcement of filler-matrix interfaces. The grafted PP chains improved the dispersion of SiO_2, and notably accelerated nucleation in crystallization. It was plausible that the grafted chains whose one chain end was pinned to SiO_2 became nuclei of the crystallization (co-crystallization between the matrix and grafted chains), thus directly bridging between the matrix and SiO_2 nanoparticles. The Young's modulus and tensile strength were most improved by the grafted PP chains at low filler contents such as 2.3 wt%, whose origin was attributed to effective load transfer to SiO_2 through the co-crystallization-mediated bridging.

1. Introduction

Polypropylene (PP) materials have been widely used for a variety of fields such as automobile parts, packaging and containers because of the advantages of low price, light weight, high melting temperature, and excellent processability & mechanical properties. They are also environmentally friendly with low production energy and high reusability/recyclability. Due to these advantages, the production and application of PP materials have continuously expanded, in which compounding with other materials has played a key role. Among a variety of PP compounds, nanocomposites containing nano-sized inorganic fillers have attracted a great attention in the last two decades because they are expected to offer properties that are not realizable with micron-sized fillers [1]

Usuki et al. reported the first successful polymer nanocomposite, Nylon 6/clay, with

excellent properties: 87°C higher heat distortion temperature and 4 times higher flexual modulus than those of the pristine polymer were achieved by adding only 5 wt% of nanoclay [2]. With nano fillers, strong interaction is achieved between a matrix polymer and fillers or between fillers at a small content (usually less than 5 wt%) of fillers. For example, percolation thresholds for nanocomposites are considerably lower than those for micro-sized composites, which facilitates much more effective reinforcement with a small amount of fillers [3]. The glass transition behavior is also modulated by a small amount of nanofillers as a result of chain confinement [4]. For semi-crystalline polymers with higher-order structures, the size of nanofiller is smaller than or comparable to the size of spherulites or lamellar morphology, and therefore the addition of nanofiller can greatly change these structures. Nitta et al. have reported that SiO_2 nanoparticles in PP depress the spherulite growth rate as the particle size decreases and as the SiO_2 content increases, while micro-sized SiO_2 (diameter of 51 μm) did not affect the spherulite growth rate [5]. Moreover, spherulites were never formed when the theoretical interparticle distance between SiO_2 nanoparticles became shorter than the end-to-end distance of PP chains. Thus, nanocomposites exhibit several aspects that are not present in the conventional composites, being expected to give a new class of high-performance materials.

A huge demand from industry has motivated enormous efforts for the development of PP-based nanocomposites. However, the results obtained until now is far from satisfactory, compared with those achieved in other polymers such as nylon 6. One of the most serious problems for PP-based nanocomposites is poor compatibility between PP and inorganic fillers: polar inorganic fillers easily form large aggregates in apolar PP matrix. Early efforts were directed to achieve homogeneous dispersion of fillers, by adding a compatibilizer and/or by an organic modification of the filler surface, for example, using silane coupling agents or organic ammonium salts for clay. Usuki et al. reported that the combination of maleic anhydride modified PP (MAPP) and organic ammonium salts resulted in siginificant exfoliation of nanoclays in PP [6]. However, the degree of mechanical reinforcement was not sufficient with respect to potentially expected reinforcement. Garcia et al. studied the effects of the filler dispersion on the mechanical properties of PP/SiO_2 nanocomposites [7]. They found that the improvement of the dispersion of SiO_2 hardly affected the tensile strength. Bikiaris et al. also showed that the addition of MAPP as a compatibilizer decreased the size of SiO_2 aggregates in PP, but only moderately improved mechanical properties [8]. Accordingly, it is concluded that good dispersion of nanofiller is not enough to realize dramatic reinforcement of PP-based nanocomposites. In addition, the most commonly used MAPP compatibilizer is known to accelerate oxidative degradation of PP [9].

In-situ composite formation is an alternative method to achieve good dispersion of

fillers without any compatibilizer and organic modification [10]. In this method, matrix polymer is synthesized in the presence of nanoparticles to automatically facilitate the dispersion of the nanoparticles. Although several authors reported good dispersion of clay, SiO_2 or carbon nanotube in PP [10-12], the mechanical properties of the resulting nanocomposites were not sufficiently investigated. It is notable that the in-situ method does not include a strategy to reinforce weak interface between PP and fillers.

One promising method to reinforce the polymer-filler interface is grafting of polymer chains to fillers, which has advantages of improved compatibility between fillers and matrix polymer and strengthed interfacial interaction through entanglements between grafted and matrix polymer chains. In addition, grafted polymer chains may decrease the aggregation tendency of fillers by their steric hinderace. Physical entanglement between grafted and matrix chains is quite attractive, since it is almost impossible to get effective chemical interaction between PP and fillers. Rong and Friedrich et al. have synthesized PP-based nanocomposites using SiO_2 nanoparticles with a variety of grafted polymer chains such as polystylene (PS), polybutylacrylate, polyvinylacrylate and so on [13-16]. However, these grafted chains did not induce large improvements of the mechanical properties of the formed nanocomposites. It is supposed that the immiscibility between PP and the grafted chains might not allow sufficient entanglement.

Based on these backgrounds, it must be preferable to graft PP chains onto nanofiller in order to acquire good miscibility with PP matrix. In employing PP itself as grafted chains, it should be noted that even PP chains can be immicible with each other when they have different primary structures. Maier et al. and Phillips reported immisivility between syndiotactic and isotactic PPs [17,18]. Silvestri et al. reported possible immisibility between isotactic and atactic PPs, depending on M_w of each component [19]. In this sence, stereo- and regio-structures of grafted PP chains should be identical to those of matrix chains. By fulfilling these requirements, resultant nanocomposites are expected to show much higer mechanical properties not only through entanglement but also through incorporation of grafted PP chains into crystallites of the matrix based on co-crystallization). Such nanocomposites with same grafted and matrix polymer chains were reported for PS and polyethylene (PE) [20-22]. In particular, a PE/PE-*g*-carbon nanotube nanocomposite showed exccellent improvements of mechanical properties by the grafted PE chains: 1.6 times higher Young's modulus and 6.9 times higher elongation at breat than those of the ungrafted nanocomposite [22]. Differently from polymers such as PS and PE, radical graft polymerization is not avairable for PP, thus PP-grafted filler is not easy to synthesize.

In this study, terminally hydroxylated isotactic PP (PP-OH) having an identical structure with matrix PP was synthesized and grafted onto SiO_2 nanoparticles, so as to

obtain the first PP-based nanocomposite having the same primary structure for the matrix and grafted PP chains. The crystallization behavior and mechanical properties of the nanocomposite were investigated by various techniques such as differential scanning calorimetry (DSC), polarized optical microscopy (POM), a tensile test and dynamic mechanical analyses (DMA).

2. Experimental

2.1. Materials

rac-[dimethylsilylenebis(4,5,6,7)-tetrahydro-1-indenyl)]zirconium dichloride was purchased from Wako pure chemical Co. Toluene and tetradecane were dried over the molecular sieve 13X before usage. Propylene gas of research grade and modified methylalumoxane (MMAO) were donated by Mitsubishi Chemical Co. and Tosoh Finechem Co., respectively. Aerosil 300 (the diameter of 7 nm and the surface area of 300 m^2g^{-1}) was employed as filler.

2.2. Synthesis of PP and PP-OH

PP used as a matrix was synthesized with *rac*-[dimethylsilylenebis(4,5,6,7)-tetrahydro-1-indenyl)]zirconium dichloride and MMAO in toluene (Al/Zr = 5000 and [Zr] = 4 μmol/L) at 0°C for 1 h under a continuous propylene flow at 1 atm. PP-OH for grafting was synthesized by hydroxylation of the chain end of PP [23]. In detail, propylene was polymerized for 1 h under the above-mentioned conditions, and then oxygen gas was bubbled in the reactor at 0°C for 1 h, followed by the addition of 1 M NaOH and 35% H_2O_2 aqueous solution. The slurry was stirred for 30 min, to accomplish terminal hydroxylation of PP. The stereoregularity, weight average molecular weight (M_w) and molecular weight distribution (MWD), and melting point of the obtained PP and PP-OH were measured by ^{13}C-NMR, high-temperature size exclusion chromatography, and differential scanning calorimetry (DSC). The synthesized PP had a high isotacticity (91 mol% in *mmmm*), M_w of 307,000 with relatively narrow MWD about 2.6, and a high melting point (T_m = 160°C). PP-OH was found to have the primary structure and thermal properties completely identical to those of the matrix PP.

2.3. Synthesis of PP-grafted SiO_2

The terminal OH group of PP-OH was reacted with the silanol groups of SiO_2 at 200°C in tetradecane for 7 h with stirring to obtain PP-grafted SiO_2 (PP-*g*-SiO_2). An adequate amount of AO-50 (donated by ADEKA Co.) was added in tetradecane to avoid thermal

degradation of PP during the reaction. The made PP-*g*-SiO_2 was washed repeatedly by hot filtration with *o*-dichlorobenzene at 145°C to completely remove ungrafted PP chains, then rinsed by methanol, and finally dried in vacuo at 60°C for 6 h. Successful grafting was confirmed by Fourier-transform infrared spectroscopy (FT-IR, FT/IR-6100, JASCO). The amount of grafted PP was evaluated by thermogravimetric analysis (TG, TG-50, METTLER), where the sample temperature was kept at 200°C for 30 min to remove physisorbed water, and then increased up to 650°C at 20°C/min. The grafted amount was estimated from the difference of the weight loss in 200-650°C between PP-*g*-SiO_2 and unmodified SiO_2. SiO_2 was also modified by octadecyltricholorosilane for the comparison (C_{18}-SiO_2). The C_{18} modification lowers the surface energy of SiO_2 as the PP grafting does, while the C_{18} group is unable to entangle and co-crystallize with the matrix PP. Thus, C_{18}-SiO_2 was utilized to exploit the relative importance between surface bulk properties (surface energy) and the molecular structure of grafted chains in the design of nanocomposites.

2.4. Preparation of nanocomposites

Nanocomposites were prepared by melt mixing using a two-roll mixer at 20 rpm. PP pellets were kneaded at 185°C for 5 min and then a specified amount of unmodified SiO_2, PP-*g*-SiO_2 or C_{18}-SiO_2 was added. The mixture was further kneaded at 185°C for additional 10 min. Thus produced nanocomposites with a variety of filler contents (0-10 wt%) were hot-pressed into sample films with the thickness of 200 μm at 230°C and 20 MPa, and then quenched at 100°C.

2.4. Instrumentation

The dispersion of SiO_2 nanoparticles in the matrix was monitored by a transmission electron microscope (TEM, Hitachi, H-7100). TEM specimens with the thickness of 100 nm were prepared by an ultramicrotome (Leica, ULTRACUTS FCS) equipped with a diamond knife (Diatome). The obtained TEM images were analyzed with a image analysis software (Image J software, NIH) to quantify the dispersion.

The crystalline structure and crystallinity of the nanocomposites were obtained by the wide-angle X-ray diffraction (Rigaku, Rint2500). Wide-angle X-ray diffraction (WAXD) measurements were performed in a reflection mode at room temperature with Cu Kα radiation operating at 40 kV and 30 mA. The scanning rate was 1°/min over 2θ of 10-30°. Sample films with a thickness of *ca.* 200 μm were used.

Isothermal crystallization was conducted at 128°C with DSC (METTELER, DSC-822). Samples were kept at 200°C for 5 min to erase a thermal history, and then cooled down to 128°C at a rate of 20 °C/min. A crystallization rate was determined as an inverse of the

half time of the crystallization (denoted as $t^{-1/2}$). A nuclear density during isothermal crystallization at 130°C was evaluated by POM (Leica, DMLB HC) equipped with an automated hot stage (METTELER, FP82HT).

Tensile tests were carried out at room temperature using a dumbbell-shaped specimen at a crosshead speed of 1.0 mm/min by a tensile tester (DAT-100, Abecks Inc.). Five measurements were performed for each sample. DMA (UBM, E4000) was conducted for the temperature dependence of oscillatory tensile moduli in the solid state (E', $\tan\delta$). Measurements were performed in the temperature range from –80 to 170°C with a heating rate of 3°C/min and the frequency of 10 Hz. The size of a sample specimen was 2 mm x 8 mm x 0.2 mm. The frequency dependence of oscillatory shear moduli in the molten state (G', G'') was measured by a parallel-and-plate rheometer (TA, AR2000ex) at 180°C with a frequency range from 100 to 0.01 rad/sec under N_2 atmosphere. The diameter of the parallel plates was 25 mm. Each measurement was performed within a linear viscoelastic region.

3. Results and discussion

3.1 Preparation of PP-g-SiO₂

The FT-IR spectrum of synthesized PP-*g*-SiO_2 was measured after careful removal of ungrafted chains with hot *o*-dichlorobenzene (Figure 1). The peaks at 2920 and 2950 cm^{-1} (corresponding to the C-H stretching vibrations for the -CH_2- and -CH_3 groups) indicate the successful grafting. TG analyses were performed to evaluate the amount of PP chains grafted on SiO_2 (Figure 2). PP-*g*-SiO_2 exhibited 12.4 wt% of the weight loss between 200 and 650°C. Referencing the weight loss of 11.1 wt% for unmodified SiO_2 in the same temperature range, the amount of the grafted PP chains was estimated as 1.3 wt%. Assuming a poreless and perfect sphere for the SiO_2 particles, the number of the grafted chains was calculated as 1 chain/particle. The amount of the octadecyl group grafted on SiO_2 was similarly obtained to be 7.5 wt%.

3.2. Dispersion State of fillers

The dispersion of unmodified SiO_2, PP-*g*-SiO_2 and C_{18}-SiO_2 in the matrix was studied by TEM (Figure 3). All the fillers formed small aggregates of 20-100 nm in the matrix. Up to the filler content of 4.0 wt%, the dispersion of PP-*g*-SiO_2 and C_{18}-SiO_2 was better than that of unmodified SiO_2. At the filler content of 10 wt%, the three kinds of fillers similarly formed large and extended aggregates. The better dispersion of PP-*g*-SiO_2 and C_{18}-SiO_2 was quantitatively confirmed by an image analysis. Table 1 shows the average areas of the

aggregates, which are 50% smaller for PP-*g*-SiO_2 and 30% for C_{18}-SiO_2. The average diameters are about 30% smaller for both PP-*g*-SiO_2 and C_{18}-SiO_2. This result proved the effectiveness of the grafting of PP chains in improving the dispersion of fillers in the PP matrix, even though the grafted amount was as small as 1 chain/particle. The observed dispersion for the three kinds of fillers might be correlated with their cohesion abilities. The modification by short alkyl groups is known to largely reduce the surface energy of SiO_2 [24], leading to better dispersion. On the other hand, the largely modified dispersion for PP-*g*-SiO_2 can be explained not only by reduction of the surface energy through the grafting, but also by steric hindrance from the grafted PP chains [13]. The way of the aggregation clearly depended on the kinds of the fillers. The aggregates of unmodified SiO_2 were larger and had an open or extended shape, while those of PP-*g*-SiO_2 and C_{18}-SiO_2 were much smaller and more compact. Bartholome et al. reported similar effects of grafted PS chains on the dispersion of SiO_2 in PS [21].

3.3. Crystalline structure and crystallization behavior

The WAXD patterns of pristine PP, PP/SiO_2, and PP/PP-*g*-SiO_2 (Figure 4) exhibited typical characteristics of the α-form crystal with the peaks of 2θ = 14.07°, 16.85°, 18.51°, 21.08° and 21.77° corresponding to (110), (040), (130), (111) and (131) reflections, respectively [25]. The other crystalline forms were never observed. Thus, SiO_2 nanoparticles and their modification had few influences on the crystalline structure of the PP matrix. The WAXD crystallinities (X_c) summarized in Table 2 were quite similar for all the samples, which allowed us to fairly compare the mechanical properties of the different samples.

Isothermal crystallization of the nanocomposites was tracked by DSC to examine influences of the fillers on the crystallization behavior of the matrix (Figure 5). Surface organic modification of fillers sometimes enhances a nucleating ability of fillers. It was found that the crystallization of PP was considerably accelerated by the addition of PP-*g*-SiO_2: the crystallization rate was 0.14 min^{-1} for PP/SiO_2 at the SiO_2 content of 2.3 wt%, while that of PP/PP-*g*-SiO_2 was 0.30 min^{-1} at the same content. The C_{18} modification of SiO_2 did not give such that significant enhancement of the nucleating ability. Thus, the high nucleating ability was originated by the molecular structure of grafted chains rather than the surface bulk nature such as surface energy.

The origin of the high nucleating ability of PP-*g*-SiO_2 was examined by POM, where the time-course increase of the nuclear densities was plotted during isothermal crystallization at 130°C (Figure 6). The nuclear density became more than twice by the addition of PP-*g*-SiO_2, indicating that the increase of the crystallization rate by PP-*g*-SiO_2 was owing to the acceleration of the nucleation rather than the acceleration of the spherulite

growth. On the other hand, unmodified SiO_2 hardly altered the nuclear density of pristine PP. Based on the result that the grafted PP chains having the same primary structure with the matrix chains significantly enhanced the nuclear density, it was plausible that the crystallization of the matrix was initiated by the grafted chains with one chain end pinned to SiO_2.

3.4. Mechanical properties

Results of Tensile tests are summarized in Figure 7 and Table 2. Unmodified SiO_2 hardly affected the Young's modulus and tensile strength at the lowest filler content, while increased these values above 4.0 wt%. The onset of the reinforcement at 4.0 wt% coincided with the formation of the percolation (described later). PP-*g*-SiO_2 showed the most notable reinforcement at the lowest content compared with unmodified SiO_2. The degree of the reinforcement became closer to that for unmodified SiO_2 at higher contents, but always larger. Only the exception was the tensile strength at 10 wt%, where the break in elongation occurred in a very early stage for PP-*g*-SiO_2. The C_{18}-modification of SiO_2 affected negatively, even though C_{18}-SiO_2 showed the better dispersion than unmodified SiO_2.

Rheological properties were evaluated to investigate interaction between the matrix and fillers. The temperature dependences of E' and tanδ are shown in Figures 8 and 9, respectively. The glass transition temperatures (T_g) determined from E'' increased about 5°C by modifications irrespective of the content and kind of the fillers (not shown). The E' values below T_g were almost the same among all the samples. The E' values above T_g were increased by the addition of both unmodified SiO_2 and PP-*g*-SiO_2 (Figure 8). However, the ways of the increases were different between the two kinds of fillers: increase of the E' value from pristine PP was about 2 times higher for PP-*g*-SiO_2 compared with unmodified SiO_2, while the advantage of PP-*g*-SiO_2 over PP/SiO_2 became much smaller at higher contents. These trends for E' are in line with the results of tensile tests. The peak intensity and area of tanδ at the glass transition generally correlate with the portion of the amorphous phase and/or the mobility of polymer chains therein [4]. Unmodified SiO_2 and PP-*g*-SiO_2 similarly reduced the peak intensity of tanδ (compared with pristine PP) (Figure 9). As shown in the X_c values of Table 2, the amorphous portion was similar among all the samples. Hence, the peak reduction by the addition of the fillers must be ascribed by reduced mobility of the amorphous chains, which is known as a confinement effect by nanoparticles [4, 26, 27]. The frequency dependences of G' and complex viscosity η^* were shown in Figure 10. A large difference was observed between pristine PP and the nanocomposites in the low frequency region (< ~0.1 rad/sec). Both G' and η^* significantly increased by the addition of the fillers.

At the filler content of 2.3 wt%, the two nanocomposites had similar *G'* values with terminal flow. However, the increase of G' was much more for unmodified SiO_2 at the higher contents. A plateau appeared instead of the terminal flow at the content over 4 wt% for unmodified SiO_2, and at the content of 10 wt% for PP-*g*-SiO_2. The appearance of the plateau in G' accompanied drastic increase of η^* by an order of magnitude. This phenomenon at higher filler contents is general for particulate nanocomposites, and indicates the formation of percolation network of fillers. The percolation has been most precisely studied for polymer/clay nanocomposites, and percolation networks through direct connections among platelets such as "edge-to-edge" or "edge-to-face" have been reported [28-30]. On the other hand, it has been considered for polymer/SiO_2 nanocmomposites that fractal structures formed by open aggregates of SiO_2 nanoparticles are responsible for the percolation [31]. As shown in Figure 3, unmodified SiO_2 formed rather open aggregates in the matrix, while PP-*g*-SiO_2 and C_{18}-SiO_2 existed as smaller and compact aggregates. The lower percolation threshold for PP/SiO_2 is clearly explained by this fact, where the percolation thresholds were between 2.3-4.0 wt% for unmodified SiO_2 and 4.0-10 wt% for PP-*g*-SiO_2.

3.5. Discussion

The obtained effects of the fillers are briefly summarized as follows. Modified SiO_2 (PP-*g*-SiO_2 and C_{18}-SiO_2) apparently improved the filler dispersion except at the highest filler content (Figure 3). PP-*g*-SiO_2 and C_{18}-SiO_2 made smaller but compact aggregates, while unmodified SiO_2 made network-like aggregates connected with each other. PP-*g*-SiO_2 showed the nucleation ability much higher than C_{18}-SiO_2 and SiO_2 (Figure 5). It was believed that the grafted PP chains initiate the crystallization of the matrix due to their lower mobility and to the same primary structure with the matrix. PP-*g*-SiO_2 showed the highest reinforcement in the tensile test at the lowest filler content (Figure 7). On the other hand, the degree of the reinforcement was similar to that of unmodified SiO_2 over 4.0 wt%. The reinforcement by C_{18}-SiO_2 was much poorer, in spite of the better dispersion of C_{18}-SiO_2 than unmodified SiO_2. SiO_2 and PP-*g*-SiO_2 similarly reduced the intensity of tanδ at the glass transition (Figure 9), indicating that the confinement of the amorphous chains by SiO_2 nanoparticles was not affected by the grafted chains. *G'* of PP/SiO_2 at low frequencies was larger than that of PP/PP-*g*-SiO_2 in the molten state (Figure 10), on the contrary to the higher Young's modulus and *E'* of PP-*g*-SiO_2 in the solid state. The disappearance of the terminal flow (corresponding to the formation of percolation network) occurred at a lower filler content for unmodified SiO_2 that for PP-*g*-SiO_2. Hereafter, the mechanistic origin of the higher reinforcement by PP-*g*-SiO_2 in the tensile tests (Figure 7) is

discussed, for which C_{18}-SiO_2 offers a useful reference.

Although the reinforcement mechanism in polymer-based nanocomposites has not been fully understood yet, the numerous efforts have identified plausible mechanisms into i) strong interfacial interaction between matrix chains and filler particles, and ii) percolation or network structures of filler particles. Load transfer to fillers based on these two mechanisms are also affected by the content, stiffness, aspect ratio, surface chemical nature and dispersion state of fillers.

The percolation threshold for PP/SiO_2 lay within the filler content 2.3-4.0 wt%. The results of tensile tests for unmodified SiO_2 were well correlated with the dependence of G' on the filler content: little reinforcement at 2.3 wt% before the percolation and sharp increases of the Young's modulus and tensile strength from 4.0 to 10 wt% after the percolation. Thus, the reinforcement for unmodified SiO_2 is believed to be mainly based on the percolation. On the other hand, PP-*g*-SiO_2 showed the most prominent reinforcement in the tensile test (compared with unmodified SiO_2) at the lowest filler content, *i.e.* before the percolation. This suggests that some strong interaction between the matrix and filler particles was responsible for the observed reinforcement. Better dispersion of fillers has been believed to result in higher reinforcement because of more homogeneously distributed load transfer to particles. In this viewpoint, PP-*g*-SiO_2 was considered to be advantageous at lower filler contents. However, as was described in introduction, good dispersion of fillers is not a sufficient condition for the reinforcement. In fact, C_{18}-SiO_2 with better dispersion than unmodified SiO_2 never showed notable improvements. These results claim the importance of the quality of the interaction between the matrix and filler particles. As in the results of DSC and POM (Figures 5 and 6), the largest difference between PP-g-SiO_2 and C_{18}-SiO_2 appeared in the nucleating ability of the fillers: the key factor for the nucleation was the molecular structure of grafted chains rather than the surface bulk natures. The considerably high nucleation ability of PP-*g*-SiO_2 suggested the crystallization of the matrix initiated from the grafted chains having the same primary structure with the matrix chains. In this way, we propose that the grafted chains are preferentially co-crystallized together with the matrix PP, and play a role of direct bridges between the matrix and filler particles for effective load transfer. This mechanism is supported by the poorer reinforcement in G' for PP/PP-*g*-SiO_2 than that of unmodified SiO_2 at the lower contents, where all crystallites were molten. The C_{18} modification was not effective for both the percolation and co-crystallization, leading to the poorest reinforcement.

A schematic image of PP/PP-*g*-SiO_2 for both the solid and molten states is drawn in Figure 11. Since the PP chains covalently grafted to SiO_2 particles preferentially co-crystallized with the matrix PP, the effective load transfer from the matrix to the fillers

occurred in the solid state, resulting in the better mechanical properties even at the lower contents much before the percolation. On the other hand, the grafted PP chains gave better filler dispersion by steric hindrance without a large increase of complex viscosity in the molten state.

4. Conclusion

In this study, a PP/SiO_2 nanocomposite having the same primary structure for the matrix and grafted PP chains was synthesized. PP-*g*-SiO_2 achieved much higher reinforcement than unmodified SiO_2, at a low filler content (2.3 wt%). We have proposed a reinforcement mechanism that the grafted PP chains trigger the crystallization of the matrix and are imparted in the lamellae of the matrix, thus directly bridging between the matrix and filler particles for effective load transfer. On the contrary, the increase of the viscosity in melt by the addition of SiO_2 was partially suppressed with the grafted PP chains. In this way, to graft PP chains having an identical structure to matrix chains can be a successful strategy to achieve significant reinforcement of PP-based nanocomposites, without sacrificing processability and light weight. Further improvements in the mechanical properties will be achieved by the optimization of the amount and structure of the grafted chains.

References

[1] Ray SS, Okamoto M (2003) Prog Polym Sci 28:1539-1641

[2] Kojima Y, Usuki A, Kawasmi M, Okada A, Fukushima Y, Kuraushi T, Kamigaito O (1993) J Mater Res 8:1185-1189

[3] Zhang Q, Archer LA (2002) Langmuir 18:10435-10442

[4] Tsagaropoilos G, Eisenberg A (1995) Macromolecules 28:6067-6077

[5] Nitta K, Asuka K, Liu B, Terano M (2006) Polymer 47:6457-6463

[6] Hasegawa N, Okamoto H, Kato M, Usuki A (2000) J Appl Polym Sci 78:1918-1922

[7] Garcia M, Vliet G, Jain S, Schrauwen BAG, Sarkissov A, Zyl WE, Boukamp B (2006) Rev Adv Mater Sci 6:169-175

[8] Bikiaris DN, Papageorgiou GZ, Pavlidou E, Vouroutzis N, Palatzoglou P, Karayannidis GP (2006) J Appl Polym Sci 100:2684-2696

[9] Morlat S, Mailhot B, Gonzalez D, Gardette JL (2004) Chem Mater 16:377-383

[10] Kaminsky W, Funck A, Wiemann K (2006) Macromol Symp 239:1-6

[11] Yang K, Huang Y, Dong JY (2007) Polymer, 48:6254-6261

[12] Funck A, Kaminsky W (2007) Compos Sci Technol 67:906-915
[13] Wu CL, Zhang MQ, Rong MZ, Friedrich K (2002) Compos Sci Technol 62:1327-1340
[14] Rong MZ, Zhang MQ, Zheng YX, Zeng HM,Walter R, Friedrich K (2001) Polymer 42:167-183
[15] Cai LF, Huang XB, Rong MZ, Ruan WH, Zhang MQ (2006) Polymer 47:7043-7050
[16] Zhou HJ, Rong MZ, Zhang MQ, Ruan WH, Friedrich K (2007) Polmer Eng Sci 47:499-509
[17] Maier RD, Thomann R, Kressler J, Mülhaupt R, Rudolf B (1997) J Polym Sci Part B: Polym Phys 35:1135-1144
[18] Phillips RA (2000) J. Polym Sci Part B: Polym Phys 38:1947-1964
[19] Silvestri R, Sgazi P (1998) Polymer 39:5871-5876
[20] Fragneaud B, Varlot KM, Montiel AG, Terrones M, Cavaillè JY (2008) Compos Sci Technol 68:3265-3271
[21] Bartholome C, Beyou E, Lami EB, Cassagnau P, Chaumont P, David L, Zydowicz N (2005) Polymer 46:9965-9973
[22] Yang BX, Pramoda KP, Xu GQ, Goh SH (2007) Adv Funct Mater 17:2062-2069
[23] Han CJ, Lee MS, Byun DJ, Kim SY (2002) Macromolecules 35:8923-8925
[24] Vidal A, Papirer E, Jiao WM, Donnet JB (1987) Chromatographia 23:121-128
[25] Farrow G (1961) Polymer 2:409-417
[26] Zhang X, Loo LS (2009) Macromolecules 42:5196-5207
[27] Wilkinson AN, Man Z, Stanford JL, Matikainen P, Clemens ML, Lees GC, Liauw CM (2006) Macromol Mater Eng, 291:917-928
[28] Okamoto M, Morita S, Kim YH, Kotaka T, Tateyama H (2001) Polymer 42:1201-1206
[29] Okamoto M, Nam PH, Maiti P, Kotaka T, Hasegawa N, Usuki A (2001) Nano Lett 1:295-298
[30] Wagener R, Reisinger TJG (2003) Polymer 44:7513-7518.
[31] Jounalt N, Vallat P, Dalmas F, Said S, Jestin J, Bocuè F (2009) Macromolecules 42:2031-2040

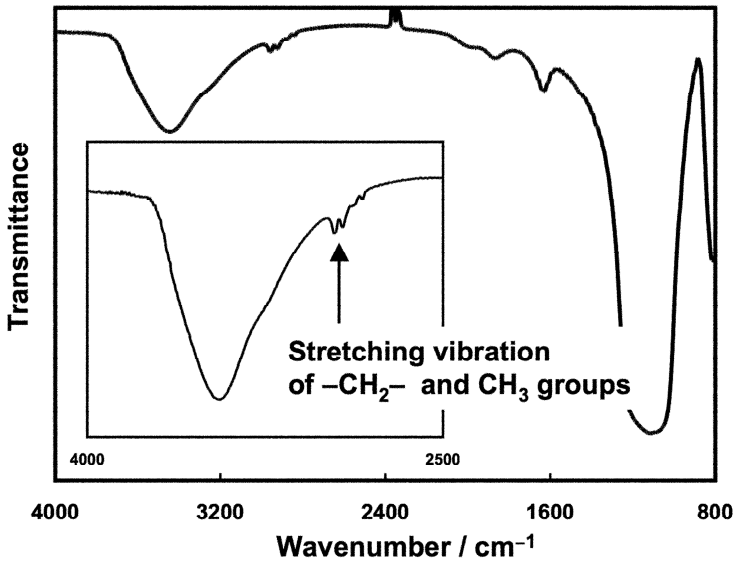

Fig. 1 IR spectrum of PP-*g*-SiO_2

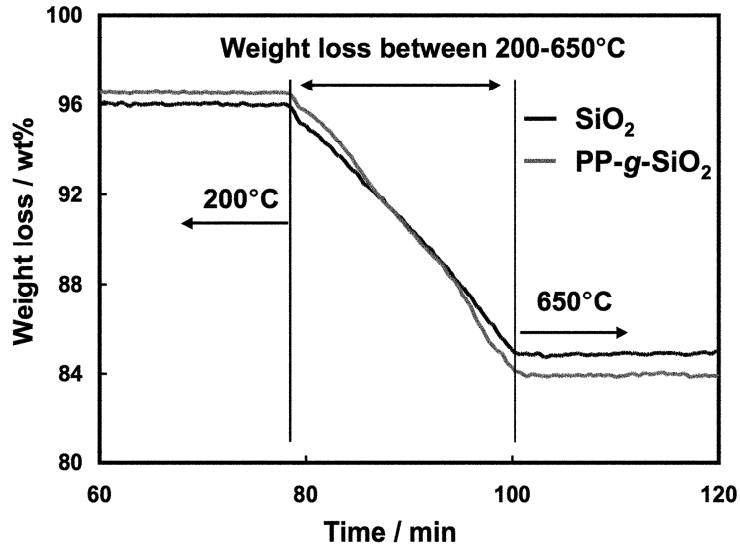

Fig. 2 TG analysis of PP-*g*-SiO_2 and unmodified SiO_2. The amount of grafted PP chains on SiO_2 was evaluated based on the weight loss between 200-650°C.

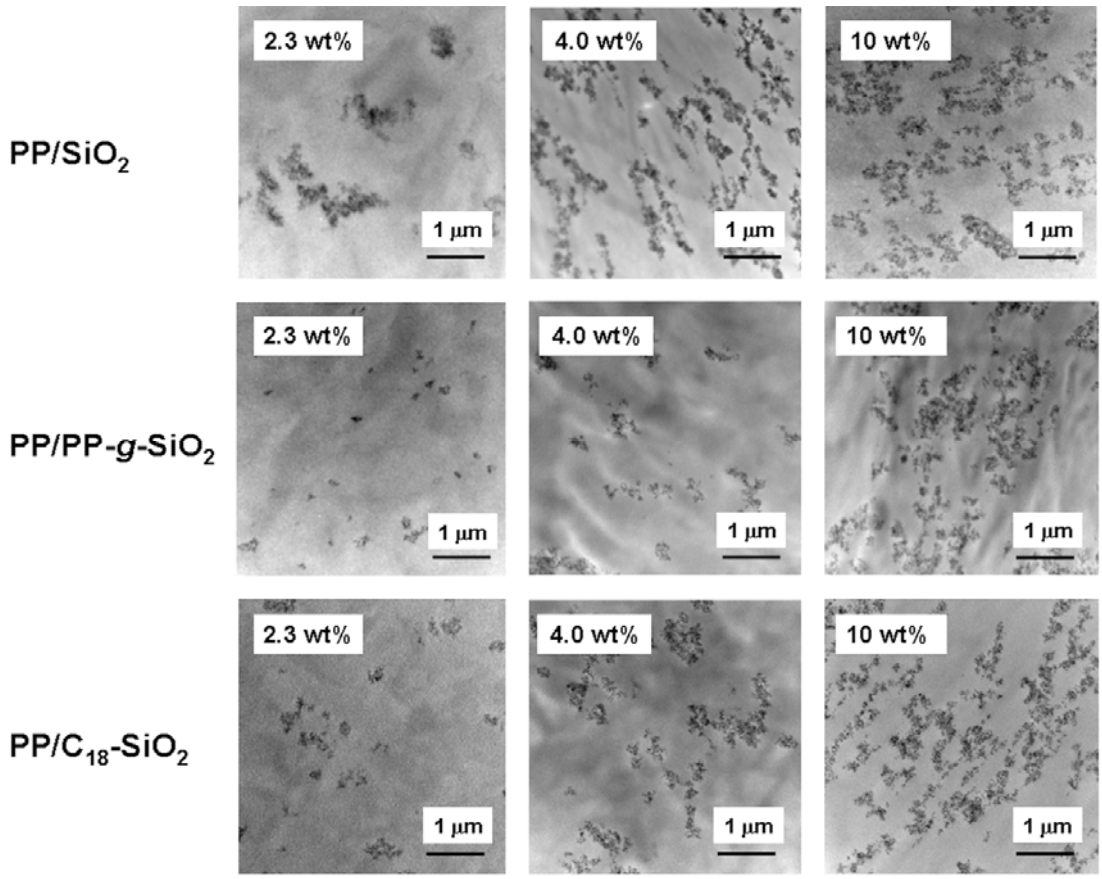

Fig. 3 TEM images of prepared PP-based nanocomposites. Filler contents were varied from 2.3 to 10 wt%.

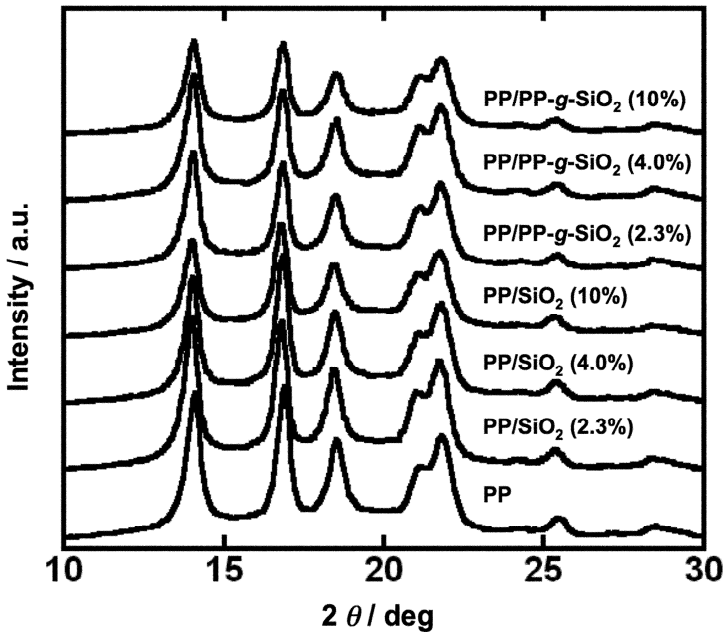

Fig. 4 WAXD patterns of pristine PP and nanocomposites. Regardless of the filler contents, all the samples showed characteristic peaks of α-form and other forms were never observed.

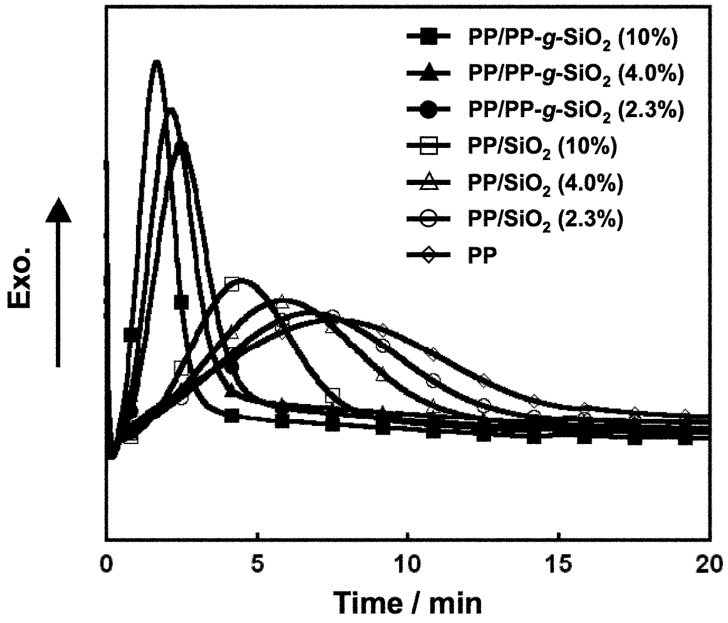

Fig. 5 DSC curves for isothermal crystallization at 128°C

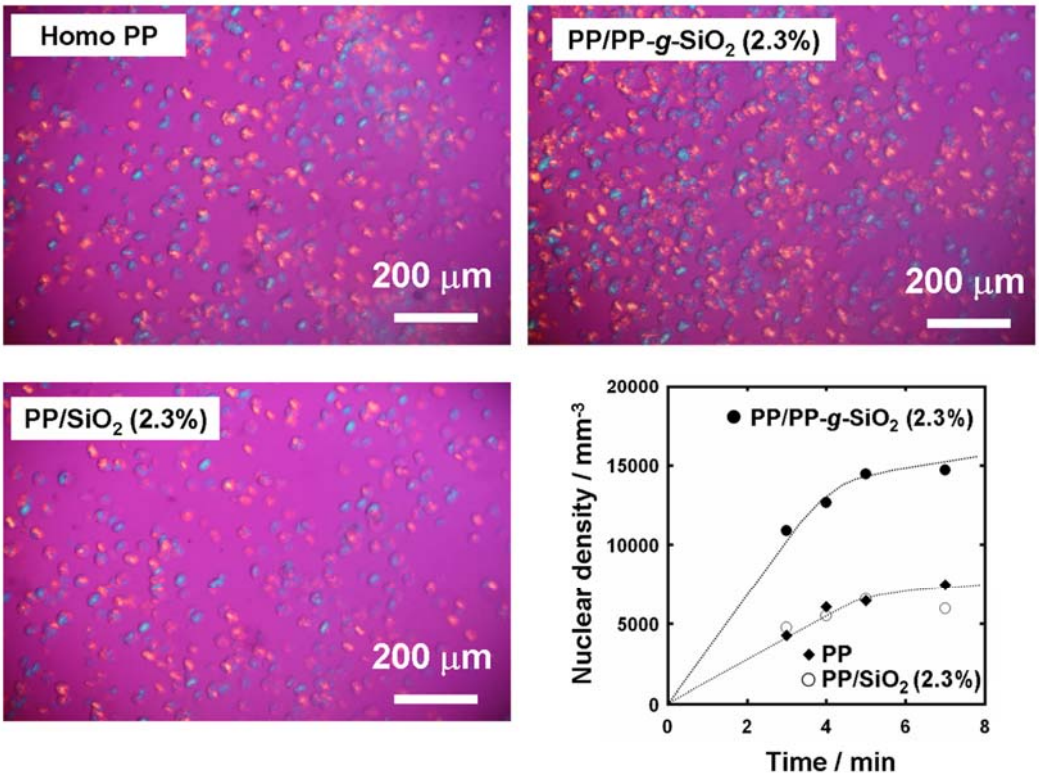

Fig. 6 POM images in isothermal crystallization at 130°C (t = 7 min) and the time dependence of the nuclear density calculated by the number of nuclei in the pictures at each time

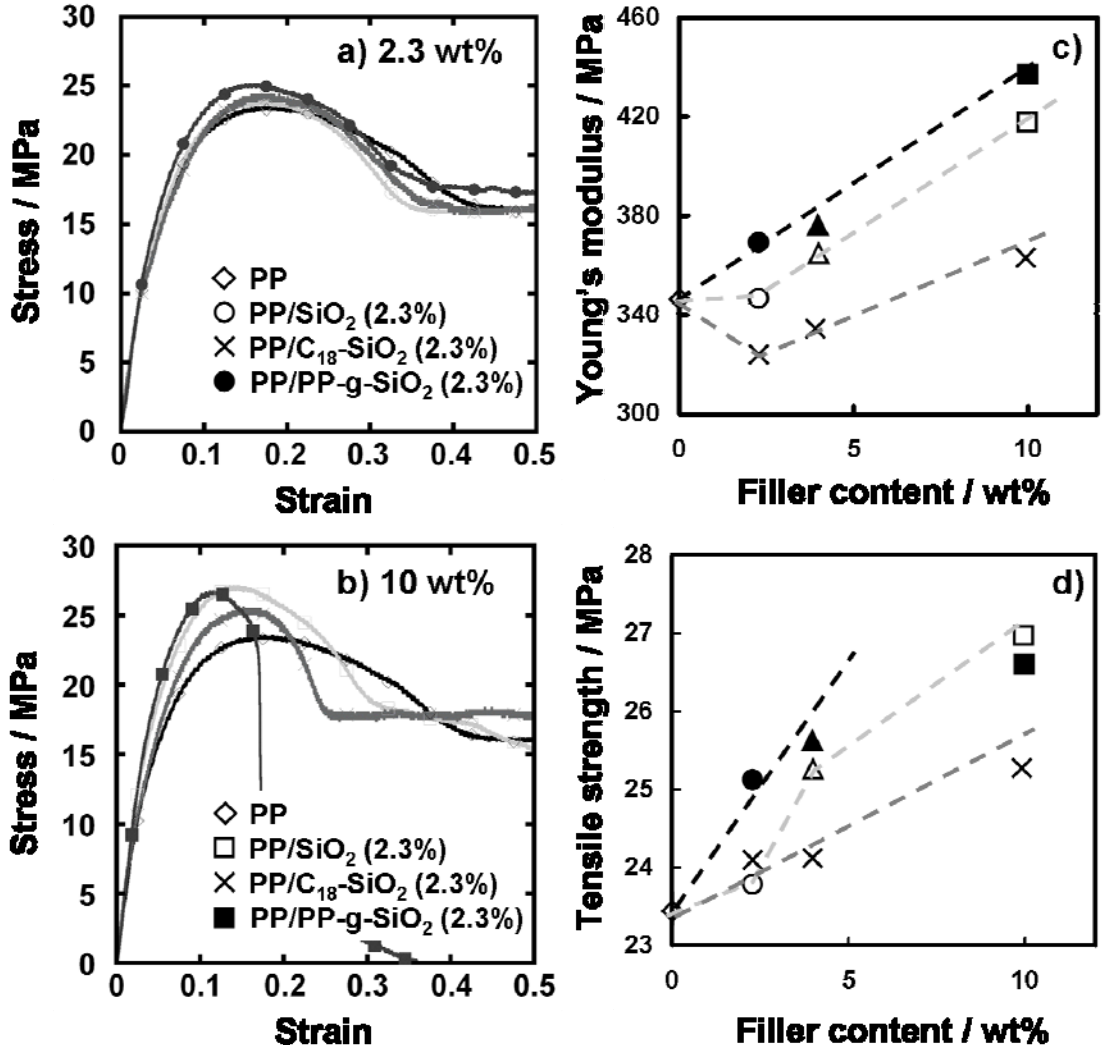

Fig. 7 Stress-strain curves (cross head speed of 1 mm/min) at the filler content of a) 2.3 wt% and b) 10 wt%. c) The Yang's modulus and d) the tensile strength were plotted against the filler content.

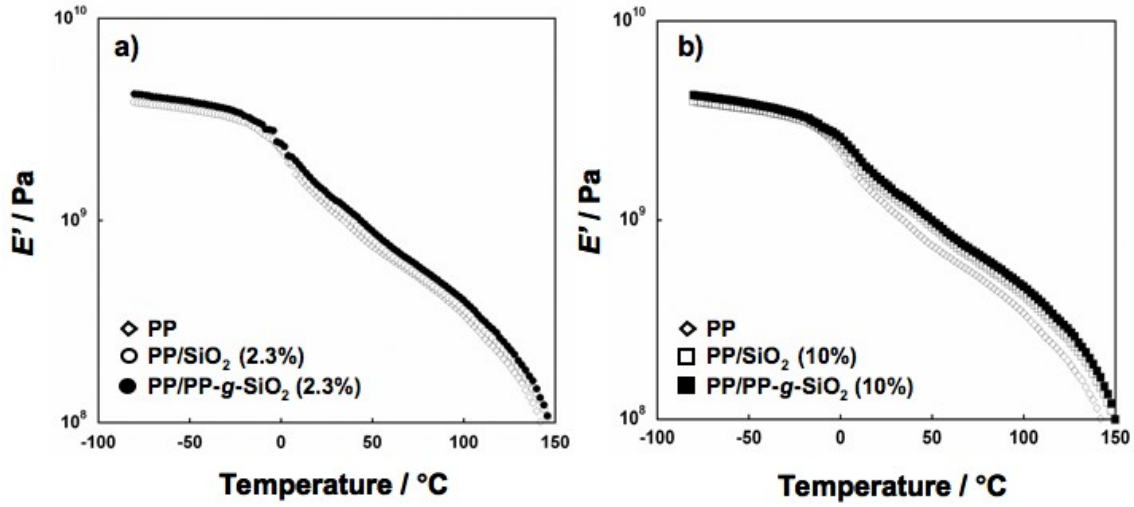

Fig. 8 Temperature dependence of tensile storage modulus *E'* for pristine PP and nanocomposites. Measurements were performed in the temperature range from –80 to 170°C with a heating rate of 3°C/min and the frequency of 10 Hz.

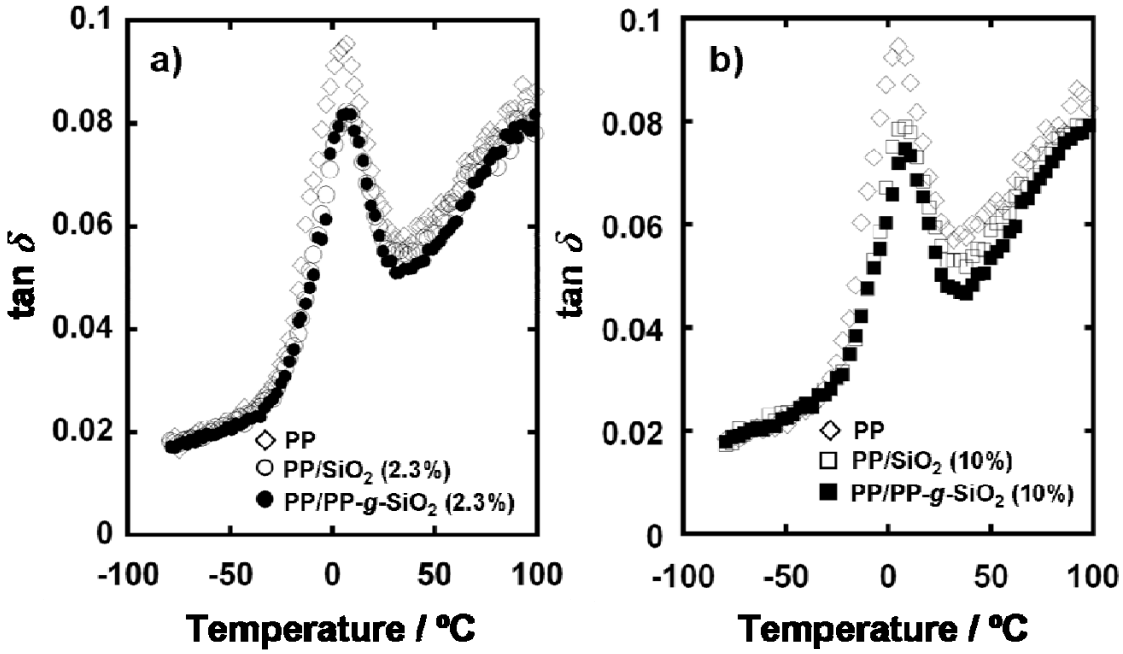

Fig. 9 Temperature dependence of loss tangent for pristine PP and nanocomposites. Measurements were performed in the temperature range from –80 to 170°C with a heating rate of 3°C/min and the frequency of 10 Hz.

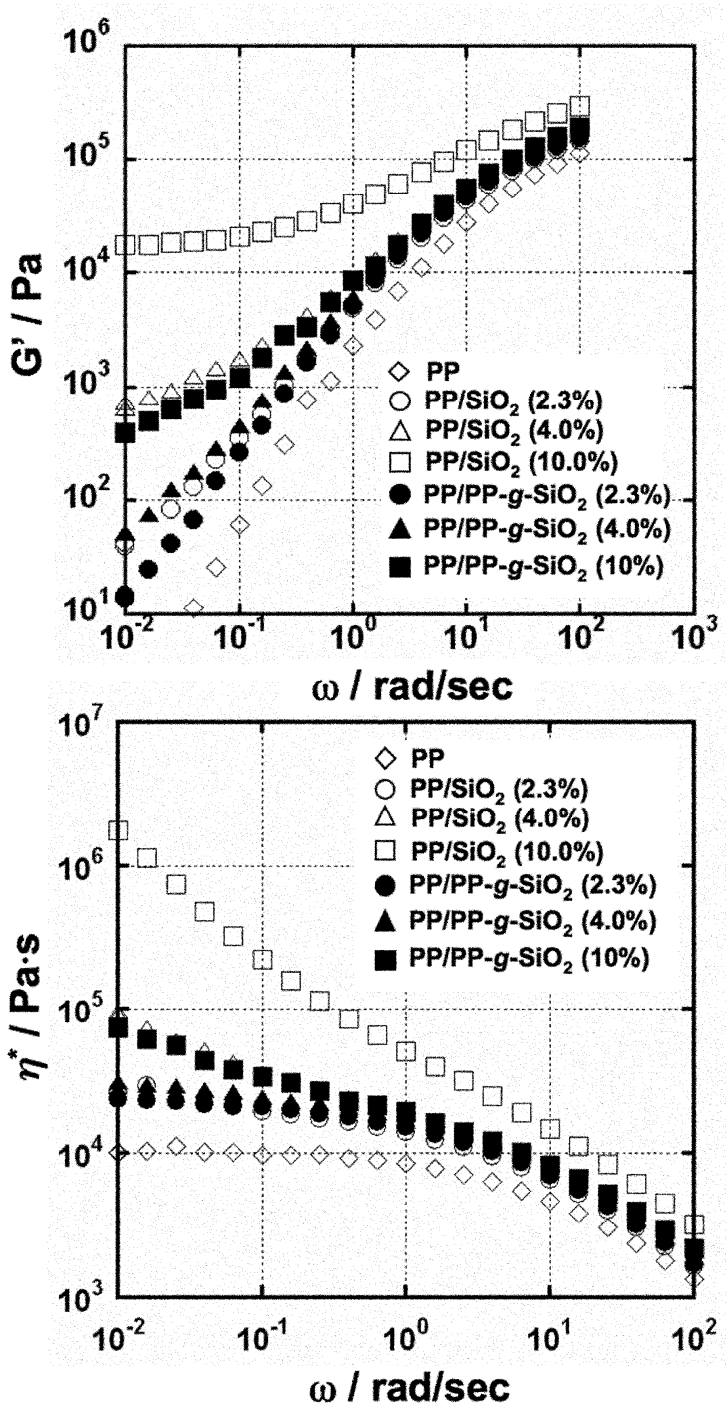

Fig. 10 Frequency dependence of shear storage modulus *G'* (upper) and (bottom) complex viscosity η^* for pristine PP and nanocomposites. Measurements were performed at 180°C with a frequency range from 100 to 0.01 rad/sec under N_2 atmosphere.

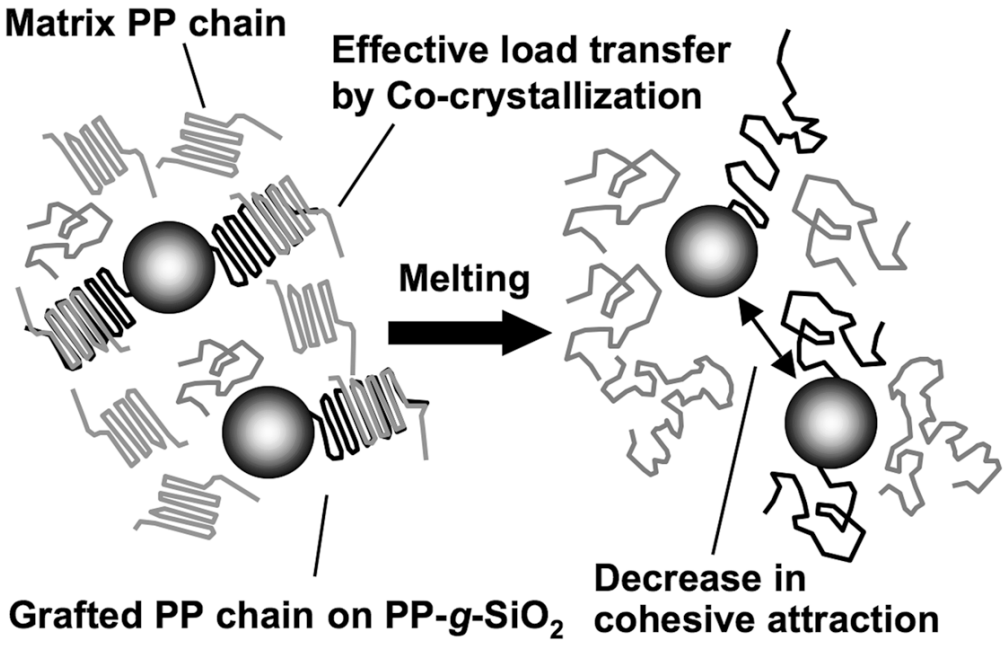

Fig. 11 Schematic image of PP/PP-*g*-SiO_2 in solid and molten states

Table 1 Size of SiO_2 aggregates[a]

Sample	Area / 10^4 nm^2	Feret diameter / nm
PP/SiO_2 (2.3%)	4.60	338
PP/SiO_2 (4.0%)	5.03	340
PP/PP-*g*-SiO_2 (2.3%)	2.15	218
PP/PP-*g*-SiO_2 (4.0%)	2.62	230
PP/C_{18}-SiO_2 (2.3%)	2.82	250
PP/C_{18}-SiO_2 (4.0%)	3.52	250

[a] Approximately 400 aggregates of SiO_2 were analyzed and averaged by a software.

Table 2 Mechanical properties and crystallinities

Sample	Young's modulus[a] / MPa	Tensile strength[a] / MPa	X_c[b] / wt%
PP	347	23.4	55.1
PP/SiO_2 (2.3%)	347	23.7	55.6
PP/SiO_2 (4.0%)	364	25.3	52.9
PP/SiO_2 (10%)	416	27.0	51.4
PP/C_{18}-SiO_2 (2.3%)	325	24.1	52.5
PP/C_{18}-SiO_2 (4.0%)	332	24.0	51.8
PP/C_{18}-SiO_2 (10%)	362	25.3	51.5
PP/PP-*g*-SiO_2 (2.3%)	369	25.0	54.3
PP/PP-*g*-SiO_2 (4.0%)	374	25.6	52.2
PP/PP-*g*-SiO_2 (10%)	439	26.7	52.2

[a] measured by tensile test, [b] determined by WAXD